Characterization of the Denatured States Distribution of Neocarzinostatin by Small-Angle Neutron Scattering and Differential Scanning Calorimetry†

D. Russo,‡,§ D. Durand,‖ P. Calmettes,‡ and M. Desmadril*,⊥

Laboratoire Léon Brillouin, CE-Saclay, 91191 Gif-sur-Yvette Cedex, France, L.U.R.E., Université de Paris-Sud, BP 34, 91898 Orsay Cedex, France, and Laboratoire de Modélisation et d'Ingénierie des Protéines−UMR 8619, Université de Paris-Sud, Bât 430, F-91405 Orsay Cedex, France

Received September 19, 2000; Revised Manuscript Received January 30, 2001

ABSTRACT: The denatured states of a small globular protein, apo-neocarzinostatin (NCS), have been characterized using several techniques. Structural properties were investigated by optical spectroscopy techniques and small-angle neutron scattering (SANS), as a function of guanidinium chloride (GdmCl) concentration. SANS experiments show that in heavy water, the protein keeps its native size at GdmCl concentrations below 2.5 M. A sharp transition occurs at about 3.6 M GdmCl, and NCS behaves like an excluded volume chain above 5 M. The same behavior is observed in deuterated buffer by fluorescence and circular dichroism measurements. For the H_2O buffer, the transition occurs with lower concentration of denaturant, the shift being about 0.6 M. 8-Anilino-1-naphthalenesulfonate (ANS) was used as a hydrophobic fluorescent probe for studying the early stages of protein unfolding. Protein denaturation modifies the fluorescence intensity of ANS, a maximum of intensity being detected close to 2 M GdmCl in hydrogenated buffer, which shows the existence of at least one intermediate state populated at the beginning of the unfolding pathway. Differential scanning calorimetry (DSC) was used to obtain thermodynamic values for NCS denaturation. The melting curves recorded between 20 and 90 °C in the presence of various GdmCl concentrations (0−3 M) cannot be explained by a simple two-state model. Altogether, the data presented in this paper suggest that before unfolding the protein explores a distribution of states which is centered around compact states at denaturant concentrations below 2 M in H_2O, and then shifts to less structured states by increasing denaturant concentrations.

Equilibrium studies of the unfolding of globular proteins provide insight into various interactions governing the stability of native structures and may provide clues as to the folding pathway. For small single-domain proteins, unfolding induced by chemical denaturants and temperature can generally be modeled, as a first approximation, by a two-state mechanism involving the native and the unfolded state (*1*). The native state is considered consisting of an ensemble of molecules with a common fold and a unique three-dimensional structure. The unfolded state is thought to be more or less a random coil with little or no regular structure (*2, 3*).

Traditionally, if the normalized transition curves for experimental measurements characterizing secondary and tertiary structures are nearly superimposable, a two-state mechanism is assumed (*4*). However, this congruence cannot be considered to be sufficient evidence to prove a two-state model, especially if there is no specific probe to characterize folding intermediates or if there is indeed a heterogeneous population of intermediates (*5, 6*). Detailed muti-parametric investigations of equilibrium folding are therefore required to improve our understanding of protein folding.

Thermodynamic characterization of the transition is of fundamental importance for understanding the mechanisms involved in folding and in the interactions that stabilize the native state (*7*). The combination of calorimetric measurements and data obtained with structural probes, such as circular dichroism or fluorescence, is a powerful approach for studying protein folding (*8−10*). Such an approach makes it possible to correlate thermodynamic and structural changes and to detect and characterize possible intermediate states.

Evidence is steadily accumulating for the existence of equilibrium and/or kinetic intermediates, even for small proteins. Although studies have mostly focused on the molten globule state (*11−14*), they have also raised new questions concerning the denatured state. For example, what defines the unfolded state, and what role do local interactions play in protein folding? Local interactions in an unfolded polypeptide chain could guide the protein toward an intermediate conformation, creating folding nuclei, thereby reducing the search through conformational space (*15−18*). Identifying the existence of folding initiation sites, as well as unfolded or partly folded intermediates, is a difficult challenge. It depends on the population of intermediate states which in

† This work was supported by the Centre National de la Recherche Scientifique and the Ministère de l'Enseignement Supérieur et de la Recherche.

* To whom correspondence should be addressed. E-mail: michel.desmadril@mip.u-psud.fr, tel: (+ 33) 1 69 15 79 75, fax: (+ 33) 1 69 85 37 15.

‡ Laboratoire Léon Brillouin, CE-Saclay.

§ Present address: Department of Chemistry and CSGI, University of Florence, Via Gino Capponi, 950121 Florence, Italy.

‖ L.U.R.E., Université de Paris-Sud.

⊥ Laboratoire de Modélisation et d'Ingénierie des Protéines−EP1088, Université de Paris-Sud.

10.1021/bi002200t CCC: $20.00
Published on Web 03/09/2001

turn depends on the equilibrium and kinetic properties of the intermediates.

The structure of the native state can be determined accurately by X-ray crystallography or nuclear magnetic resonance in solution, but it is more difficult to describe the denatured states. Structural information from scattering techniques coupled with the results of polymer theory (*19*) can provide a deep and clear understanding of the properties of the unfolded states. Whereas NMR is useful to determine residual structures in unfolded states (*20*, *21*), scattering techniques can provide simultaneous information about molecular weight, size, shape, internal conformation of flexible scatterers, and interactions existing between scatterers. Small-angle scattering of either neutrons or X-rays (SANS or SAXS)[1] has been successfully used to determine the structural properties of various denatured states of proteins (*22*−*31*). The structural information provided by SAXS experiments has been used to characterize intermediates not only during the folding of proteins (*32*−*35*) but also during the folding of other biomolecules such as RNA (*36*).

We further investigated protein folding using a model protein, neocarzinostatin (NCS), the fold of which is characteristic of a large protein family: the immunoglobulin fold. Neocarzinostatin is a natural antibiotic chromoprotein consisting of 117 amino acid residues and a labile chromophore (*37*). The structure of apo-NCS essentially consists of a seven-stranded antiparallel β-barrel which forms a cavity in which the chromophore binds to form the active complex. It contains two disulfide bridges, between cysteinyl residues 37−47 and 88−93, which contribute to the high stability of the protein.

Various complementary techniques were used in an attempt to detect possible intermediate states and to describe in detail the various states of the protein. In particular, we used a fluorescent hydrophobic molecular probe, 8-anilino-1-naphthalenesulfonate (ANS), and differential scanning calorimetry (DSC) to detect compact intermediates. The structural properties of the native state, the compact denatured states, and the strongly unfolded states are described. Circular dichroism and fluorescence spectroscopy were used to study the variations of secondary and tertiary structures of NCS. Small-angle neutron scattering was used to follow the changes in size of the protein molecule and DSC to determine the stability of the various intermediate states.

MATERIALS AND METHODS

Sample Preparation. Recombinant apo-NCS (mass = 11 079 g/mol) was expressed in *Escherichia coli* and purified as previously described (*38*). All measurements were carried out in 60 mM phosphate buffer, pH 7.0, in which the electrostatic interactions were almost screened out as shown by a series of SAXS experiments with various phosphate concentrations. Buffers were prepared with both light and heavy water (H_2O and D_2O) because neutron scattering measurements were performed within D_2O. The use of D_2O for neutron experiments increases the contrast between the protein and the solvent, and minimizes incoherent scattering from hydrogen atoms. Before each experiment, the purified protein was extensively dialyzed against the appropriate buffer. The chemical denaturant was guanidinium chloride (GdmCl) which was deuterated as previously described (*22*). Deuterated solutions of NCS were prepared with great care to prevent contamination with hydrogen atoms. Each sample was prepared at least 12 h before the experiment, to obtain denatured states at equilibrium. The protein concentration of the samples was determined from the absorbance at 280 nm, using an extinction coefficient $\epsilon = 1.2$ cm^2 mg^{-1}.

Optical Spectroscopy Techniques. Tryptophan fluorescence was excited by light at a wavelength of 295 nm, to maximize the quantum efficiency. Emission spectra were recorded between 300 and 400 nm at constant bandwidth (2 nm), using an SLM 8000C fluorimeter (Aminco). The inner optical path of the sample was 1 cm. Measurements were performed with a wavelength increment of 0.2 nm and an integration time of 0.2 s. The protein concentration was 10 μM and the temperature 12 °C. All spectra were corrected for instrument response and for the Raman scattering of the solvent.

ANS, a fluorescent hydrophobic probe, was used to monitor the solvent exposure of the apolar residues in the protein matrix. The concentration of ANS was 10 times larger than that of the protein (10 μM). The excitation wavelength was 350 nm, and emission was recorded between 350 and 500 nm at constant bandwidth (2 nm). Data were corrected for the solvent effect on the intrinsic ANS fluorescence intensity by subtracting ANS fluorescence spectra in the absence of protein, for each denaturant concentration. All spectra were corrected for instrument response.

Circular dichroism in the far-ultraviolet range was determined with a Mark V dichrograph (Jobin Yvon, France). CD spectra were recorded between 190 and 260 nm for the native protein and between 210 and 240 nm for the protein in GdmCl solutions, due to the strong absorbance of the denaturant at shorter wavelengths. The optical path length of the samples was 0.5 mm. The wavelength increment was 0.5 nm and the integration time 0.8 s. Ten measurements were performed for each sample and averaged. The protein concentration was 30 μM and the temperature 12 °C.

Circular dichroism and fluorescence were determined after 12 h of incubation at 12 °C in various concentrations of GdmCl solution. Ultrapure GdmCl was obtained from Pierce; denaturant concentration was checked by refractometry, using the relationship provided by Nozaki (*39*). Transition curves were constructed by plotting either the variation in ellipticity at 223 nm or the wavelength of maximum fluorescence emission as a function of denaturant concentration.

Thermodynamic analysis was performed using the model of the linear dependence of the free energy change, ΔG, on denaturant concentration, x, as described by Pace (*40*):

$$\Delta G(x) = \Delta G_0 - mx \qquad (1)$$

Assuming that the linear dependence of the free energy change on denaturant concentration observed in the transition region can be extrapolated to zero denaturant concentration, ΔG_0 represents the standard variation of free energy in the absence of denaturant and m a constant proportional to the increase in the degree of exposure of the protein to the solvent on denaturation. Analysis of the data was performed

[1] Abbreviations: ANS, 8-anilino-1-naphthalenesulfonate; CD, circular dichroism; DSC, differential scanning calorimetry; GdmCl, guanidinium chloride; NCS, apo-neocarzinostatin; R_g, radius of gyration; SANS, small-angle neutron scattering; SAXS, small-angle X-ray scattering; UV, ultraviolet.

using an equation derived from eq 1, taking into account the baselines and the transition region:

$$y(x) = y_n + s_n x = \left\{\frac{e^{(\Delta G_0 - mx)/RT}}{1 + e^{(\Delta G_0 - mx)/RT}}\right\}[A + (s_d - s_n)x] \quad (2)$$

where $y(x)$ is the experimental signal in the presence of x molar GdmCl and y_n is the signal of the native form. s_n and s_d are the solvent effects on the native and denatured protein signal, respectively, and A is the amplitude of the transition. Equation 2 was fitted to the experimental data using a simplex procedure based on the Nelder & Mead algorithm (*41*). Standard errors were calculated for a 95% confidence level.

Small-Angle Neutron Scattering. The SANS experiments were carried out at Laboratoire Léon Brillouin with the PACE spectrometer. This apparatus is equipped with 30 concentric annular detectors and a central circular detector measuring the scattered and transmitted beam intensities, respectively. For most experiments, the incident neutrons had a wavelength $\lambda = 0.8$ nm, and the sample to detector distance, d, was 2.4 m. These conditions yield momentum transfers of 0.2−1.0 nm^{-1}. The momentum transfer is defined as $q = (4\pi/\lambda) \sin(\theta/2)$, where θ is the scattering angle. A different set of conditions ($\lambda = 0.4$ nm, $d = 1.3$ m) was also used for native and fully unfolded proteins to obtain scattering curves up to a momentum transfer of 3.6 nm^{-1}.

All the samples were contained in fused-silica cells with an inner path length of 5 mm. Each measurement took about 6 h. Sample scattering spectra were corrected for solvent scattering and for the nonuniformity of the detector response by normalization to the incoherent scattering for a water sample in a cell of 1.0 mm path length. Finally, a constant was subtracted from the spectra to correct for incoherent scattering due to the nonexchangeable hydrogen atoms (H) of the protein. Absolute calibration was achieved by measuring the intensity of the neutron beam with the detectors used to record the scattering spectra. The experiments were carried out at 15 °C in D_2O solutions with a NCS concentration of 5 mg cm^{-3}.

The coherent scattering spectrum, $I(q,c)$, of a solution depends on the solute concentration c. The following approximation, which is only valid for small values of q, may describe this relationship:

$$\frac{cMK^2}{N_A I_{coh}(q,c)} \cong \frac{1 + 2A_2Mc + 3A_3Mc^2 + ...}{1 + 2B_2Mc + 3B_3Mc^2 + ...}\left[\frac{1}{P(q)} + 2B_2Mc + 3B_3Mc^2 + ...\right] \quad (3)$$

In this equation, N_A is Avogadro's number and M is the molar mass (g/mol) of the solute. K is the mean relative contrast of the molecule to the solvent defined as

$$K = \rho_p v - \rho_s v_p$$

where ρ_p and ρ_s are the mean neutron scattering-length densities (cm^{-2}) of the scatterers and solvent, respectively. v is the specific volume (cm^3 g^{-1}), and v_p is the partial specific volume (cm^3 g^{-1}) of the solute.

Finally, $P(q)$ is the structure factor of a single molecule. It is defined such as $P(0) = 1$ and is proportional to the scattering spectrum the molecule would give at infinite dilution. All the coefficients A_i and B_i are related to the potential of the interactions between i molecules. The coefficients A_i are the ith virial coefficients of the solution, and the B_i depend on the correlation distance of the interactions (*42*). These interactions depend on the molecules themselves and on the properties of the solvent. The values of A_i and B_i can be determined from measurements carried out at various protein concentrations. The coefficients B_i are not necessarily identical to the virial coefficients A_i, as can be inferred from the Zimm approximation (*43*).

For compact scatterers, such as globular proteins, the apparent value of the radius of gyration, $R_g(c)$, may be inferred from the spectra using the Guinier approximation (*44*):

$$I(q,c) \cong I(0,c) \exp\left\{-\frac{[q^2R_g^2(c)]}{3}\right\} \quad (4)$$

For almost spherical particles, this approximation remains valid up to $qR_g(c) \approx 1.3$. We used this relationship to determine the apparent value of the radius of gyration of native and nativelike conformations of NCS. For an unfolded chain, the scattering spectrum is much better described by the Debye function (*45, 46*):

$$\frac{I(q,c)}{I(0,c)} = \frac{2(x - 1 + e^{-x})}{x^2} \quad (5)$$

where $x = [qR_g(c)]^2$. This expression holds for $[qR_g(c)] \leq 3$ (*46*). For solutions containing several different populations (native, denatured, and possibly intermediate), we have shown (*42*) that the Debye function gives more realistic values than the Guinier approximation for the apparent radius of gyration, provided that $q \leq 1.4/R_g(c)$.

It is often necessary to correct the apparent values of forward scattered intensity, $I(0,c)$, and radius of gyration, $R_g(c)$, for the concentration effect. This can be done by performing measurements at various solute concentrations, c, and extrapolating the data to $c = 0$. According to eq 3, the forward scattered intensity is given by

$$I(0,c) \cong I(0,0)(1 + 2A_2Mc + 3A_3Mc^2 + \cdots)^{-1} \quad (6)$$

and the apparent radius of gyration by

$$R_g^2(c) \cong R_g^2(0)(1 + 2B_2Mc + 3B_3Mc^2 + \cdots)^{-1} \quad (7)$$

Differential Scanning Calorimetry. DSC experiments were carried out using a MC2 calorimeter (MicroCal, USA). The cell volume was 1.22 cm^3. Protein samples (1 mg cm^{-3}) were studied for a temperature range of 15−90 °C and GdmCl concentrations up to 5 M, equilibrated in either H_2O or D_2O. Scans were performed with two different heating rates (0.5 and 1 K min^{-1}) to check that measurements were not significantly affected by the unfolding kinetics. Samples were extensively dialyzed against the denaturing buffer, and both buffer and samples were thoroughly degassed before measurement. The dialysis buffer was used as a reference for measurements. We assessed the reversibility of NCS unfolding, using H_2O buffers at various pH values and in the

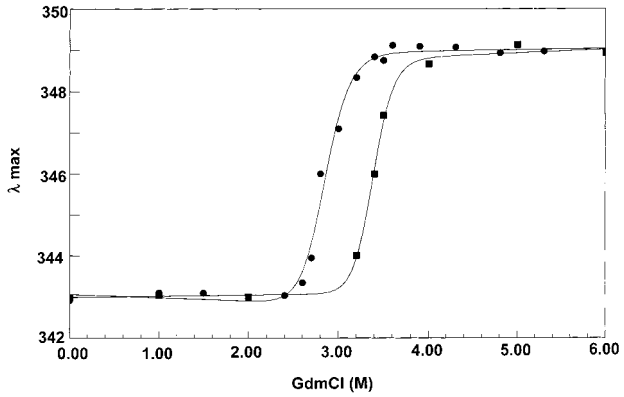

FIGURE 1: Unfolding transition curve at 12 °C, assessed by the variation of the position of the maximum of fluorescence intensity (excitation at 295 nm) as a function of denaturant concentration. Fluorescence spectra corrected for instrument response were recorded between 310 and 450 nm at constant bandwidth (2 nm) after 12 h of incubation of 10 μM NCS at 12 °C in various denaturant concentrations in 60 mM phosphate buffer, pH 7.0, either in H_2O (●) or in D_2O (■). The continuous line represents the best fit of the data according to a two-state transition using eq 2.

presence of GdmCl, by rescanning a denatured sample after cooling at 15 °C for 0.5 h.

The heat capacity of the solvent alone was subtracted from that of the protein sample. These corrected data were analyzed using a cubic spline as the baseline in the transition. Thermodynamic parameters, ΔH_{cal} and ΔH_{vH}, were determined by fitting the following equation to the data:

$$\Delta C_p(T) = \frac{K_D(T)\Delta H_{cal}\Delta H_{vH}}{[1 + K_D(T)]^2 RT^2} \quad (8)$$

where K_D is the equilibrium constant for a two-state process. ΔH_{cal} is the measured enthalpy, corresponding to

$$\Delta H_{cal} = \int_{T_I}^{T_F} C_p(T)\, dT \quad (9)$$

and ΔH_{vH} is the enthalpy calculated on the basis of a two-state process. If the measured transition corresponds to a two-state process, the values of the two enthalpies, ΔH_{cal} and ΔH_{vH}, are equal. Values for the $\Delta H_{cal}/\Delta H_{vH}$ ratio other than 1 imply the presence of intermediates or a multimolecular process (*47*).

RESULTS AND DISCUSSION

Equilibrium Transition Induced by GdmCl. (A) Fluorescence and Circular Dichroism. NCS denaturation was studied as a function of GdmCl concentration in both H_2O and D_2O to assess the influence of isotopic exchange on protein unfolding (*48*) and to make possible direct comparison of the fluorescence and CD results with those of the SANS experiments carried out in only D_2O.

Figure 1 shows the wavelength, λ_{max}, corresponding to the maximum fluorescence intensity of NCS in H_2O and D_2O as a function of denaturant concentration. Upon unfolding, the emission maximum of tryptophan shifts from 343 to 349 nm. Based on the structure of native NCS (*37*), the high value of the fluorescence wavelength of the native protein is due to the high level of exposure of the two tryptophans to the solvent. In H_2O, the transition occurs between 2 and 4 M GdmCl, with a midpoint transition, C_M, of 2.85 M. In D_2O buffer, the protein is more stable, the transition being shifted to higher denaturant concentrations and more cooperative. The protein remains nativelike up to 3 M GdmCl and unfolds between 3 and 4 M GdmCl with a C_M of 3.40 M. In both buffers, the protein lost its tertiary structure at 4 M GdmCl, leading to the complete exposure of the two tryptophan residues to the solvent.

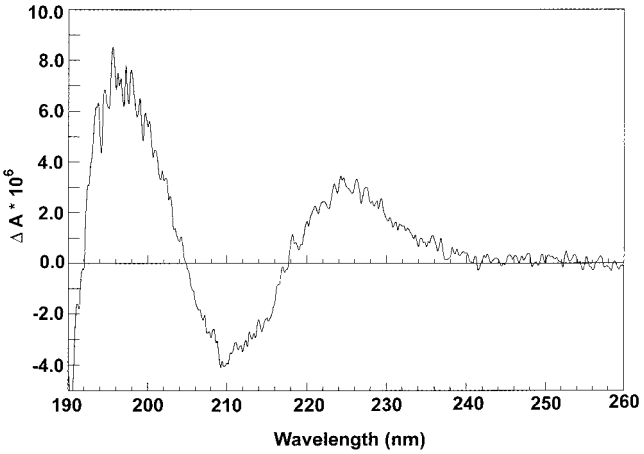

FIGURE 2: Far-UV CD spectrum of native NCS in H_2O. The spectrum of a 30 μM sample, in 60 mM phosphate buffer, pH 7.0, was recorded at 12 °C from 190 to 260 nm and subtracted from the buffer baseline. The optical path length of the cell was 0.5 mm.

The unfolding transition observed by fluorescence may be described as a two-state process. In this approximation, the calculated Gibbs free energy of unfolding, ΔG_0, and the proportionality constant, *m*, in eq 1 are 9.9 ± 0.5 kcal mol^{-1} and 3.5 ± 0.4 kcal mol^{-1} M^{-1} in H_2O and 11.7 ± 0.5 kcal mol^{-1} and 3.4 ± 0.1 kcal mol^{-1} M^{-1} in D_2O, respectively.

The far-UV CD spectrum of NCS is unusual for a predominantly β-sheet protein (Figure 2). The spectrum of the native state displays two clear maxima. The first occurs between 190 and 205 nm and is typical of a β structure. The second, between 210 and 230 nm, may result from constraints in the polypeptide backbone, such as bent folds and turns (*49*−*51*). The presence of disulfide bridges connecting cysteine residues located very close together, at positions 37−47 and 88−93, may account for such a signal reported as "not typical" secondary structures (*38*).

The absorbance of GdmCl makes it impossible to follow the CD signal in the 195 nm region. We therefore studied the variation of circular dichroism at 223 nm as a function of denaturant concentration (Figure 3). Previous studies have shown that transitions induced by temperature and monitored at 195 and 223 nm give the same results (data not shown). It is therefore reasonable to assume that the data reported in Figure 3 provide reliable information about the breakdown of secondary structure during the unfolding process. In the H_2O buffer, NCS retains a nativelike conformation for concentrations of GdmCl up to 2 M and completely lost its secondary structure at 3.3 M GdmCl. The concentration of denaturant at mid-transition is C_M = 2.8 M. For the D_2O buffer, the transition is shifted toward higher denaturant concentrations, with C_M = 3.4 M GdmCl. In both buffers, a single transition was observed. In the approximation of a two-state transition, the Gibbs free energy of unfolding, ΔG_0, and the *m* values were found to be ΔG_0 = 7.2 ± 0.7 kcal

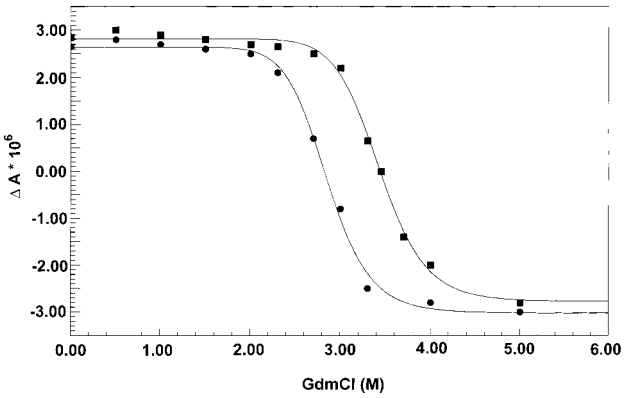

FIGURE 3: Unfolding transition curve at 12 °C, assessed by the variation of the ellipticity at 223 nm as a function of denaturant concentration. CD spectra were recorded between 210 and 240 nm after 12 h of incubation of 30 μM NCS at 12 °C in various denaturant concentrations in 60 mM phosphate buffer, pH 7.0, either in H_2O (●) or in D_2O (■). The continuous line represents the best fit of the data according to a two-state transition using eq 2.

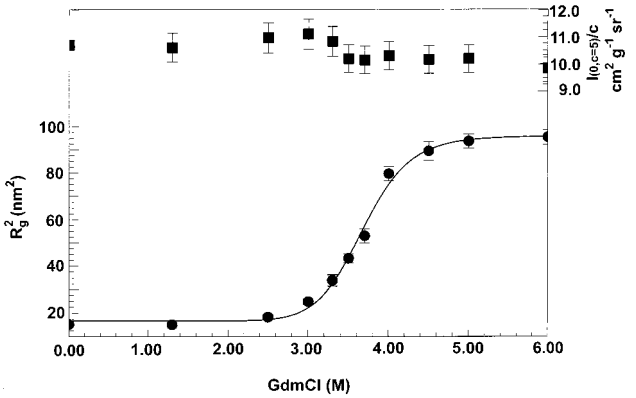

FIGURE 4: Unfolding transition curve assessed by the variation of the square of the apparent radius of gyration, $R_g(c)$ (●), as a function of denaturant concentration (left scale). The continuous line represents the best fit of the data according to a two-state transition using eq 2. The experiments were carried out at 15 °C in D_2O, 60 mM phosphate buffer, pD 7.0, with an NCS concentration of 5 mg cm^{-3} incubated for 12 h in the various denaturant concentrations. The experimental values $I(0,c = 5\text{ mg cm}^{-3})$ are reported on the right scale (■).

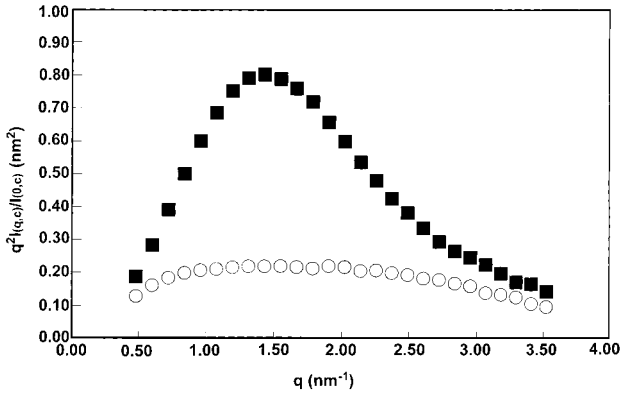

FIGURE 5: Kratky plot $q^2I(q,c)/I(0,c)$ vs q of NCS in the native (■) and fully unfolded state in 5 M GdmCl (○) (protein concentration: 20 mg cm^{-3}). The scattering profile of the native protein is bell-shaped, characteristic of a globular object, whereas it displays a nearly flat shape in the unfolded state.

mol^{-1} and $m = 2.5 \pm 0.2$ mol^{-1} M^{-1} for NCS in H_2O and $\Delta G_0 = 7.8 \pm 0.7$ kcal mol^{-1} and $m = 2.3 \pm 0.2$ kcal mol^{-1} M^{-1} in D_2O.

Both CD and fluorescence signals give rise to symmetric transition curves that may be analyzed as a two-state transition, but slight differences are observed in the parameters describing these transitions, suggesting that the denaturation process may involve intermediates.

We observe an apparent enhancement of the protein stability in D_2O. While this effect has been described for many other proteins (*52*−*54*), the exact nature of this enhancement of stability is not known. Makhatadze et al. (*55*) propose that the change in enthalpy of unfolding due to water isotopic substitution can be rationalized by changes in hydration of the buried nonpolar groups. However, other studies suggest that polar surface exposition as well as hydrogen bonds should also be considered in order to understand the solvent isotope effect on enthalpy (*56*, *57*). A global analysis of the thermal and chemical denaturation would give further information on the factors contributing to the enhancement of stability of NCS, but the deviation from a two-state process prevents such an analysis.

(B) Neutron Scattering. (i) Equilibrium Transition. In protein unfolding processes, at least two species, the native and fully unfolded proteins, are present simultaneously in the solution. For a very dilute solution containing n different species, the measured mean radius of gyration, $R_g(0)$, is given by

$$R_g^2(0) = \sum_{i=1}^{n} f_i R_{g,i}^2(0) \qquad (10)$$

where f_i and $R_{g,i}(0)$ are the proportion and the radius of gyration of species i, respectively.

In practice, the radius of gyration of the solution was measured at a finite protein concentration, c. Figure 4 shows the squared equilibrium value of the apparent radius of gyration $R_g(c)$ of NCS ($c = 5$ mg cm^{-3}) as a function of GdmCl concentration. In the figure is also shown the dependency of the $I(0,c)/c$ value on GdmCl concentration. The theoretical values of $I(0,c)/c$ can be computed from eq 3 for $q = 0$, using a value of 0.72 cm^3 g^{-1} for υ_p derived following the approach of Kharakoz (*58*) and taking into account the dependency of the contrast K and the virial coefficient A_2 values on GdmCl concentration. The calculated value for $c = 5$ mg cm^{-3} is nearly constant for the various denaturant concentrations and close to 10 cm^2 g^{-1} sr^{-1}. The good agreement of theoretical and experimental values of $I(0,c)/c$ rules out any aggregation process. This is also underlined by the excellent agreement, even at the smallest q values, which was observed between the experimental scattering curves and their fits by the appropriate equation (eqs 4 and 5).

For $c = 5$ mg cm^{-3}, the native NCS has an apparent radius of gyration of 1.25 ± 0.02 nm. The size of the protein remains similar to that of the native protein up to a concentration of 3 M GdmCl, beyond which it begins to increase significantly. At 5 M GdmCl and above, NCS is completely unfolded, and its scattering spectrum (Figure 5) is similar to that of a chain with excluded volume interactions, as explained in Russo et al. (*59*). Its apparent radius of gyration is $R_g(c) = 3.06 \pm 0.06$ nm. The transition midpoint is at $C_M = 3.6$ M, and the denaturation curve may

be described as a simple two-state transition with $\Delta G_0 = 7.5 \pm 0.2$ kcal mol^{-1} and $m = 2.0 \pm 0.1$ kcal mol^{-1} M^{-1}. However, these results are slightly biased by concentration effects, because the measured value of the radius of gyration depends on concentration if the interactions between particles are not negligible. To evaluate the effect of protein concentration on the shape of the transition curve for the radius of gyration, we studied interactions between NCS molecules in the native and unfolded states.

(ii) Protein−Protein Interactions. SANS experiments were carried out as a function of protein concentration for both the native state and the completely unfolded state obtained in 5 M GdmCl. The values of the actual radius of gyration, $R_g(0)$, and the second virial coefficient, A_2, were inferred from the data using eqs 7 and 6, respectively.

For the native NCS, we obtained $A_2 = (2.7 \pm 0.1) \times 10^{-4}$ cm^3 mol g^{-2} and $R_g(0) = 1.29 \pm 0.03$ nm. This value for the radius of gyration is consistent with that calculated from the atomic coordinates using the program CRYSON (*60*). The second virial coefficient, A_2, is related to intermolecular forces consisting mainly of hard-core, repulsive electrostatic, and attractive van der Waals interactions. It is useful to compare the experimental value of A_2 with the value obtained with a simple hard sphere potential. For neutral molecules, the second virial coefficient is related to the radius of gyration by the expression:

$$A_2 = \Psi 4\pi^{3/2} N_A R_g^3(0)\ \mathrm{M}^{-2} \qquad (11)$$

where ψ depends on the nature of the solute. For hard spheres, $\psi = 1.619$. Substituting the experimental value of $R_g(0)$ into eq 11 gives $A_2 = (4 \pm 0.3) \times 10^{-4}$ cm^3 mol g^{-2}, close to the experimental value. Thus, in 60 mM phosphate D_2O buffer, the repulsive Coulombic interactions compensate for the attractive van der Waal interactions.

The protein in a solution containing 5 M GdmCl has a second virial coefficient $A_2 = (6 \pm 0.9) \times 10^{-4}$ cm^3 mol g^{-2}, and the radius of gyration of the unfolded protein is $R_g(0) = 3.3 \pm 0.1$ nm. Equation 11 is valid for linear molecules, such as synthetic polymers and unfolded proteins. ψ varies with the length and stiffness of the chain and with the strength of excluded volume interactions (*61*). In particular, $\psi = 0$ for an ideal chain. If there are excluded volume interactions, ψ is positive. Its value is close to 0.23 for a flexible chain of infinite length. With the experimental values of A_2 and $R_g(0)$, eq 11 gives $\psi = 0.16 \pm 0.06$, consistent with the value expected for a relatively short excluded volume chain (*61*). This implies that unfolded NCS molecules interact preferentially with the solvent, rather than with itself, or with other protein molecules. The unfolded protein molecules are therefore completely solvated.

In conclusion, the difference between $R_g(0)$ and R_g(5 mg cm^{-3}) is very small in the native state and less than 7−8% in the unfolded state. We can therefore assume that the variation of the radius of gyration measured at $c = 5$ mg cm^{-3} as a function of GdmCl concentration is not significantly different from that of the actual radius.

ANS Binding Experiments. Figure 6 shows the effect of GdmCl concentration on the ANS fluorescence intensity at 475 nm. This experiment was carried out in H_2O. The native and completely denatured protein interacts weakly with ANS whereas a large increase of intensity is observed between 1 and 3 M GdmCl with a maximum close to 2 M. This reflects changes in the ANS environment. If the protein is native, the fluorescent probe is in a polar environment, and its quantum efficiency is low. If the protein is sufficiently destabilized by the denaturant, internal interactions become weaker, enabling ANS to enter the protein matrix and come into contact with the hydrophobic residues. At high denaturant concentrations, the secondary and tertiary structures are completely destroyed, as indicated in Figures 1 and 3, and all the hydrophobic residues are exposed to the solvent. In this case, ANS remains in a polar environment, and its fluorescence decreases. This behavior is typical of proteins with an unfolding pathway more complex than a simple two-state transition for which ANS is always exposed to the solvent. This change in fluorescence intensity indicates that relatively compact intermediate states are present in mildly denaturing conditions and are populated at the beginning of the unfolding pathway.

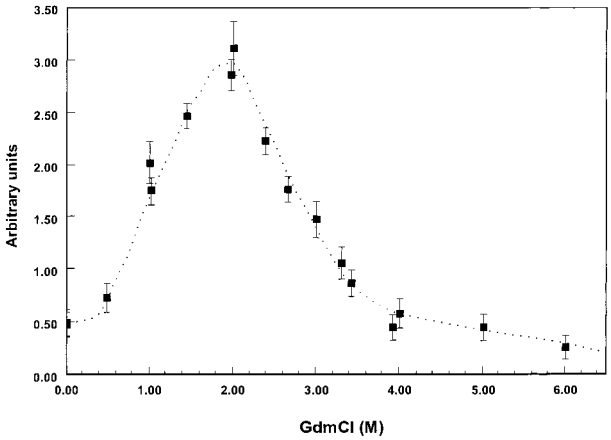

FIGURE 6: Effect of GdmCl concentration on ANS fluorescence intensity at 475 nm (excitation at 350 nm) in the presence of 10 μM NCS, in 60 mM phosphate buffer, pH 7.0, H_2O. Spectra were acquired at a constant bandwidth (2 nm) and corrected for instrument response. Data were corrected for the solvent effect on the intrinsic ANS fluorescence intensity.

DSC Experiments. DSC melting curves were recorded for NCS in various H_2O buffer conditions. Without denaturant, pH and ionic strength were changed such that the heat capacity of unfolding could be estimated in various conditions. For pH values between 5.0 and 7.0 (data not shown), the thermal denaturation of NCS was highly reversible. Thus, for temperatures ranging from 20 to 90 °C, the first and the second calorimetric recordings were similar in shape, with 95% recovery of the denaturation enthalpy. No dependence of melting temperature on protein concentration ($1 \leq c \leq 5$ mg cm^{-3}) or heating rate was observed.

At pH 7.0, the midrange temperature of the transition is $T_M = 68.6 \pm 0.1$ °C. Using a two-state model, the enthalpy was estimated to be about 106 kcal mol^{-1}. However, a better fit was obtained if the calorimetric enthalpy, ΔH_{cal}, and the van't Hoff enthalpy, ΔH_{vH}, were not assumed to be equal. In this case, $\Delta H_{cal} = 97.3$ kcal mol^{-1} and $\Delta H_{vH} \cong 115$ kcal mol^{-1}. This is consistent with the hypothesis that the unfolding transition is not a two-state process, but instead involves intermediates. However, as the reversibility of the transition was only 95%, some aggregation may account for the slight deviation in the value of the $\Delta H_{vH}/\Delta H_{cal}$ ratio from unity.

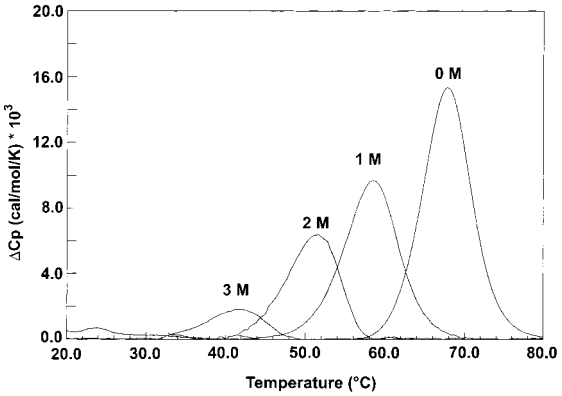

FIGURE 7: Corrected partial molar excess heat capacity of a 3 mg cm^{-3} NCS solution in 60 mM phosphate buffer, pH 7.0, H_2O, for various GdmCl concentrations (scan rate 1 K min^{-1}).

Table 1: Thermodynamic Parameters of Heat Denaturation of Apo-NCS in H_2O and D_2O, in the Presence of Various Concentrations of GdmCl[a]

sample	T_{m1} (°C)	ΔH_{cal1} (kcal mol^{-1})	ΔH_{vH1} (kcal mol^{-1})	T_{m2} (°C)	ΔH_{cal2} (kcal mol^{-1})	ΔH_{vH2} (kcal mol^{-1})
0 M/H_2O	68.6	97	115			
1 M/H_2O	58.3	86	99			
2 M/H_2O	49.3	32	76	54	37	120
3 M/H_2O	39.4	10	90	43	6	140
0 M/D_2O	71.8	98	119			
2 M/D_2O	49.2	30	102	53	22	140
3 M/D_2O	39.8	15	85	44	15	125

[a]Analyses were performed taking into account either one non-two-state transition (ΔH_{cal1} and ΔH_{vH1}) or two non-two-state transitions (ΔH_{cal1} and ΔH_{vH1}, ΔH_{cal2} and ΔH_{vH2}). ΔH_{cal}, calorimetric enthalpy; ΔH_{vH}, van't Hoff enthalpy.

DSC measurements were also carried out for the various states of NCS, for GdmCl concentrations of 1, 2, and 3 M, i.e, in the same concentration range as for ANS binding experiments.

As expected, protein stability is reduced by the presence of GdmCl (Figure 7). The amplitude and temperature of the maximum of the heat capacity peak decrease with increasing concentrations of denaturant. In addition to this overall destabilization, the peak became clearly asymmetric at denaturant concentrations beyond 1 M (Table 1). Full reversibility was observed, excluding the possibility that this phenomenon was due to aggregation (*62*). These results indicate that intermediate states are present in the range of the denaturant concentrations used and are consistent with the results of ANS fluorescence measurements showing that the interior of the protein becomes more accessible to the solvent as the GdmCl concentration increases.

The thermal transitions cannot be analyzed using a two-state model. At least two transitions, of non-two-state model, are required to account for the results obtained at concentrations of 2 and 3 M GdmCl. The thermodynamic parameters describing these transitions are given in Table 1.

These observations may be accounted for either by the presence in the solution of a single intermediate species with structural properties changing almost continuously with temperature or by the presence of two or more different intermediate species in thermodynamic equilibrium.

We also carried out a similar experiment in heavy water, with 0, 2, and 3 M GdmCl in D_2O. Complete reversibility was observed at pD = 7.0. Unlike that in the H_2O solution, the melting curve obtained in the D_2O solution in the absence of GdmCl at pD = 7.0 cannot be approximated by a simple two-state model and needs the two distinct values for ΔH_{cal} and ΔH_{vH} to be correctly fitted. The following results are obtained: $T_M = 71.8$ °C, $\Delta H_{cal} = 97.8$ kcal mol^{-1}, and $\Delta H_{vH} \cong 120$ kcal mol^{-1}. In the presence of various denaturant concentrations, a similar analysis to that performed for data obtained in H_2O buffer was carried out (Table 1). This analysis suggests that the intermediates have the same characteristics as those in H_2O. We also checked that two consecutive recordings made with 2 M GdmCl in D_2O had similar profiles.

Finally the melting curve of a sample containing 5 M GdmCl was also recorded to check that the protein was completely unfolded at this denaturant concentration. Heat capacity showed no transition peak as a function of temperature.

CONCLUSION

To a first approximation, each of the transition curves, obtained by fluorescence, circular dichroism, or small-angle scattering measurements, may apparently be described by a two-state process involving only a folded and an unfolded state. However, this approximation gives different values of the Gibbs free energy of unfolding, depending on the probe used. This indicates that the two-state model cannot describe the entire unfolding process of NCS. Thus, although each transition curve has a sigmoid shape similar to that of a two-state transition, it probably corresponds to an average of two or more successive transitions, or to an almost continuous unfolding phenomenon. Further evidence supporting this notion was provided by ANS binding experiments: between 1 and 3 M GdmCl, there is at least one intermediate state that binds ANS, this or these intermediates being mainly populated close to 2M GdmCl.

Although ANS binding experiments and SANS measurements were performed in different solvents, they provide information about the degree of compactness of these intermediates. In comparison with experiments performed in H_2O, the transition in D_2O is shifted by about 0.6 M to a higher denaturant concentration (Figures 1 and 3). Taking into account this shift, SANS data imply that at a denaturant concentration of 1.9 M in H_2O, the value of the apparent radius of gyration R_g is close to that of the native one (Figure 4). Thus, ANS binds to an intermediate state that has structural characteristics close to those of the native state: it is compact, with a native secondary structure but with a slightly different tertiary structure because the hydrophobic regions are accessible to the ANS probe.

This feature is typical of a molten globule state, but the information obtained is insufficient to determine whether a distribution of intermediate states or a well-defined molten globule is present in the sample in this range of GdmCl concentrations. Consequently, complementary experiments were required.

We therefore performed differential scanning calorimetry experiments. As expected, for GdmCl concentrations between 1 and 3 M, the DSC recordings do not correspond to a two-state transition, indicating that at least one intermediate species is present in these denaturing conditions. Subsequent

analysis of these melting curves clearly showed that even a three-state transition could not describe the denaturation process. Therefore, more than one intermediate state is required to account for these results. This is consistent with the hierarchical cooperative model proposed by Griko to account for the denaturation process of α-lactalbumin (*63*). In this model, the denatured state is represented as a distribution of substates with various degrees of residual structures. This distribution accounts for the difficulty encountered in trying to identify a unique intermediate state, and the absence of a well-defined population of this intermediate.

The observed intermediate states probably correspond merely to a distribution of states which is, at the lowest denaturant concentrations, centered around compact states with significant residual structure. At high denaturant concentrations, this distribution shifts to less structured states until it reaches the excluded volume conformation of the strongly unfolded states. As unfolding conditions increase, NCS protein gradually and continuously changes its structure until the hydrophobic interactions are completely destabilized, destroying the β-barrel structure in a cooperative manner. Then, the unfolding process continues until the excluded volume conformation is reached.

Previous studies have suggested that the various proteins sharing the immunoglobulin-like fold also share common features in their folding process (*64*). This could suggest that the intermediates observed in these studies are specific to the immunoglobulin-like fold. However, as observed for other immunoglobulin-like proteins such as the fibronectin type III module (*65*), similar folding pathways do not imply that the same intermediates are present, since homologous proteins can display either two- or three-state transitions. This may be due to the nature of the distribution of intermediates states, the properties of the distribution differing from one protein to another.

ACKNOWLEDGMENT

We thank Dr. Charles Robert for carefully reading the manuscript. We are indebted to Dr. N. Rosato for the use of its fluorimeter for ANS experiments.

REFERENCES

1. Jackson, S. E. (1998) *Folding Des. 3*, R81−91.
2. Smith, L. J., Fiebig, K. M., Schwalbe, H., and Dobson, C. M. (1996) *Folding Des. 1*, R95−106.
3. Kataoka, M., and Goto, Y. (1996) *Folding Des. 1*, R107−114.
4. Tanford (1968) *Adv. Protein Chem. 23*, 121−282.
5. Ptitsyn, O. B. (1994) *Protein Eng. 7*, 593−596.
6. Baldwin, R. L., and Rose, G. D. (1999) *Trends Biochem. Sci. 24*, 77−83.
7. Privalov, P. L. (1979) *Adv. Protein Chem. 33*, 167−241.
8. Makhatadze, G. I., and Privalov, P. L. (1992) *J. Mol. Biol. 226*, 491−505.
9. Ibarra-Molero, B., Laladze, V. V., Makhatadze, G. I., and Sanchez-Ruiz, J. M. (1999) *Biochemistry 38*, 8138−8149.
10. Zhou, Y., Hall, C. K., and Karplus, M. (1999) *Protein Sci. 8*, 1064−1074.
11. Ptitsyn, O. B., Pain, R. H., Semisotnov, G. V., Zerovnik, E., and Razgulyaev, O. I. (1990) *FEBS Lett. 262*, 20−24.
12. Griko, Y. V. (2000) *J. Mol. Biol. 297*, 1259−1268.
13. Chakraborty, S., and Peng, Z. (2000) *J. Mol. Biol. 298*, 1−6.
14. Dalessio, P. M., and Ropson, I. J. (2000) *Biochemistry 39*, 860−871.
15. Zerovnik, E., Jerala, R., Virden, R., Kroon Zitko, L., Turk, V., and Waltho, J. P. (1998) *Proteins: Struct., Funct., Genet. 32*, 304−313.
16. Wong, K. B., Clarke, J., Bond, C. J., Neira, J. L., Freund, S. M., Fersht, A. R., and Daggett, V. (2000) *J. Mol. Biol. 296*, 1257−1282.
17. Zhou, B., Tian, K., and Jing, G. (2000) *Protein Eng. 13*, 35−39.
18. Receveur, V., Garcia, P., Durand, D., Vachette, P., and Desmadril, M. (2000) *Proteins: Struct., Funct., Genet. 38*, 226−238.
19. des Cloizeaux, J., and Jannink, G. (1990) in *Polymers in solution: their modelling and structure*, Carendon Press, Oxford, U.K.
20. Kortemme, T., Kelly, M. J., Kay, L. E., Forman-Kay, J., and Serrano, L. (2000) *J. Mol. Biol. 297*, 1217−1229.
21. Russell, B. S., Melenkivitz, R., and Bren, K. L. (2000) *Proc. Natl. Acad. Sci. U.S.A. 97*, 8312−8317.
22. Calmettes, P., Roux, B., Durand, D., Desmadril, M., and Smith, J. C. (1993) *J. Mol. Biol. 231*, 840−848.
23. Petrescu, A. J., Receveur, V., Calmettes, P., Durand, D., Desmadril, M., Roux, B., and Smith, J. C. (1997) *Biophys. J. 72*, 335−342.
24. Kataoka, M., Kuwajima, K., Tokunaga, F., and Goto, Y. (1997) *Protein Sci. 6*, 422−430.
25. Damashun, G., Damaschun, H., Gast, K., and Zirwer, D. (1998) *Biochemistry (Moscow) 63*, 259−275.
26. Panick, G., Malessa, R., Winter, R., Rapp, G., Frye, K. J., and Royer, C. A. (1998) *J. Mol. Biol. 275*, 389−402.
27. Hagihara, Y., Hoshino, M., Hamada, D., Kataoka, M., and Goto, Y. (1998) *Folding Des. 3*, 195−201.
28. Segel, D. J., Fink, A. L., Hodgson, K. O., and Doniach, S. (1998) *Biochemistry 37*, 12443−12451.
29. Pollack, L., Tate, M. W., Darnton, N. C., Knight, J. B., Gruner, S. M., Eaton, W. A., and Austin, R. H. (1998) *Proc. Natl. Acad. Sci. U.S.A. 96*, 10115−10117.
30. Kamatari, Y. O., Ohji, S., Konno, T., Seki, Y. I., Soda, K. I., Kataoka, M., and Akasaka, K. (1999) *Protein Sci. 8*, 873−882.
31. Konno, T., Kamatari, Y. O., Tanaka, N., Kamikubo, H., Dobson, C. M., and Nagayama, K. A. (2000) *Biochemistry 39*, 4182−4190.
32. Segel, D. D., Bachmann, A., Hofrichter, J., Hodgson, K. O., Doniach, S., and Kiefhaber, T. (1999) *J. Mol. Biol. 288*, 489−499.
33. Arai, M., Ikura, T., Semisotnov, G. V., Kihara, H., Amemiya, Y., and Kuwajima, K. (1998) *J. Mol. Biol. 275*, 149−162.
34. Segel, D. J., Eliezer, D., Uversky, V., Fink, A. L., Hodgson, K. O., and Doniach, S. (1999) *Biochemistry 38*, 15352−15359.
35. Kojima, M., Tanokura, M., Maeda, M., Kimura, K., Amemiya, Y., Kihara, H., and Takahashi, K. (2000) *Biochemistry 39*, 1364−1372.
36. Russell, R., Millett, I. S., Doniach, S., and Herschlag, D. (2000) *Nat. Struct. Biol. 7*, 367−370.
37. Adjadj, E., Quiniou, E., Mispelter, J., Favaudon, V., and Lhoste, J. M. (1992) *Eur. J. Biochem. 203*, 505−511.
38. Heyd, B., Lerat, G., Adjadj, E., Minard, P., and Desmadril, M. (2000) *J. Bacteriol. 182*, 1812−1818.
39. Nozaki, Y. (1970) *Methods Enzymol. 26*, 43−50.
40. Pace, C. N. (1986) *Methods Enzymol. 131*, 266−280.
41. Press, W. H., Flannery, B. P., Tenkolsky, S. A., and Vetterling, W. T. (1986) in *Numerical Recipes*, Cambridge University Press, Cambridge, U.K.
42. Russo, D. (2000) Thèse de l'Université Paris-Sud.
43. Receveur, V., Durand, D., Desmadril, M., and Calmettes, P. (1998) *FEBS Lett. 426*, 57−61.
44. Guinier, A., and Fournet, G. (1955) in *Small Angle Scattering of X-rays*, Wiley-Interscience, New York.
45. Debye, P. (1944) *J. Appl. Phys. 15*, 338−342.
46. Rawiso, M., Duplessix, R., and Picot, C. (1987) *Macromolecules 20*, 630−648.
47. Freire, E. (1995) *Methods Enzymol. 259*, 144−168.
48. Kuhlman, B., and Raleigh, D. P. (1998) *Protein Sci. 7*, 2405−2412.

49. Woody, R. W. (1994) *Eur. Biophys. J. 23*, 253−262.
50. Dufton, M. J., and Hider, R. C. (1983) *CRC Crit. Rev. Biochem. 14*, 113−171.
51. Reid, K. L., Rodriguez, H. M., Hiller, B. J., and Gregoret, L. M. (1998) *Protein Sci. 7*, 470−479.
52. Bonnete, F., Madern, D., and Zaccai, G. (1994) *J. Mol. Biol. 244*, 436−447.
53. Kuhlman, B., Boice, J. A., Fairman, R., and Raleigh, D. P. (1998) *Biochemistry 37*, 1025−1032.
54. Goto, Y., Hagihara, Y., Hamada, D., Hoshino, M., and Nishii, I. (1993) *Biochemistry 32*, 11878−11885.
55. Makhatadze, G. I., Clore, G. M., and Gronenborn, A. M. (1995) *Nat. Struct. Biol. 2*, 852−855.
56. Kuhlman, B., and Raleigh, D. P. (1998) *Protein Sci. 7*, 2405−2412.
57. Oas, T. G., and Toon, E. J. (1997) *Adv. Biophys. Chem. 6*, 1−52.
58. Kharakoz, D. P. (1997) *Biochemistry 36*, 10276−10285.
59. Russo, D., Durand, D., Desmadril, M., and Calmettes, P. (2000) *J. Phys. Chem. B 278*, 520−521.
60. Svergun, D. I., Richard, S., Koch, M. H., Sayers, Z., Kuprin, S., and Zaccai, G. (1998) *Proc. Natl. Acad. Sci. U.S.A. 95*, 2267−2272.
61. Yamakawa, H., Abe, F., and Einaga, Y. (1993) *Macromolecules 26*, 1898−1904.
62. Sanchez-Ruiz, J. M., Lopez-Lacomba, J. L., Cortijo, M., and Mateo, P. L. (1988) *Biochemistry 27*, 1648−1652.
63. Griko, Y. E., Freire, P., and Privalov, P. (1994) *Biochemistry 33*, 1889−1899.
64. Clarke, J., Cota, E., Fowler, S. B., and Hamill, S. J. (1999) *Struct. Folding Des. 7*, 1145−1153.
65. Cota, E., and Clarke, J. (2000) *Protein Sci. 9*, 112−120.

BI002200T